Cement and Concrete Research 41 (2011) 872–881

Contents lists available at ScienceDirect

Cement and Concrete Research

journal homepage: http://ees.elsevier.com/CEMCON/default.asp

Effects of air voids on ultrasonic wave propagation in early age cement pastes

Jinying Zhu *, Seong-Hoon Kee, Dongyeop Han, Yi-Te Tsai

Department of Civil, Architectural, and Environmental Engineering, the University of Texas, Austin, TX 78712–0273, USA

ARTICLE INFO

Article history:
Received 6 August 2010
Accepted 15 April 2011

Keywords:
Cement hydration
Air voids
Ultrasonic waves
Shear waves
Setting time

ABSTRACT

The objective of this paper is to investigate effects of air voids on ultrasonic wave propagation in fresh cement pastes, and relate ultrasonic wave parameters to cement setting times. First, Biot's theory was used to analyze wave propagation in poroelastic media containing air bubbles. Then, in the experimental study, both the compressional (P) and shear (S) waves were monitored in cement pastes with different water/cement ratios (w/c = 0.4 and 0.5) and various air void content (0.1%–5.3% by cement paste volume). Experimental results indicated that existence of air bubbles in cement paste significantly decreases the P wave velocity, but has little effect on the shear wave propagation. Further analysis shows that the shear wave velocity corresponding to the Vicat initial setting times is a relatively constant value for the investigated air content range. This study shows the potential of using shear waves to monitor setting and hardening process of cement.

1. Introduction

Many test methods have been developed to characterize early age properties of cementitious materials, which include Vicat needle [1], rheological measurement [2], chemical shrinkage [3], electrical conductivity [4] and ultrasonic methods [5–10], etc. These methods measure mechanical, chemical and electrical properties during stiffening and hardening processes of cementitious materials. However, the microstructural development and fluid-to-solid transition, or the solidification process, will be better described by methods that measure mechanical properties of cementitious materials.

Ultrasonic waves have been widely used to characterize and evaluate hardened concrete based on the relationship between wave velocity and the mechanical properties (Young's modulus) of elastic solids. Since 1980s, research using ultrasonic waves to investigate early age properties of cement pastes and concrete has grown rapidly. Elastic and viscoelastic properties of cementitious materials can be obtained from ultrasonic wave velocity [3–6,11–13], attenuation [4] or reflection [9] measurements.

In 1980s, Keating et al. [6] investigated ultrasonic longitudinal (P) wave propagation in fresh cement pastes. They showed that at very early age, the P wave velocity V_P is governed by the fluid phase before the solid phase becomes interconnected. They also found that presence of air bubbles strongly influences the P wave velocity and attenuation. Sayers and Dahlin [12] confirmed the findings by comparing ultrasonic wave signals in de-aired and as-mixed cement pastes, and used Biot's theory to analyze wave propagation in saturated porous media. Since then, many studies have been focused on correlating the P wave velocity V_P and the Vicat initial setting time [7,13–17]. Researchers have developed different methods to identify initial setting time of cementitious materials based on certain features on the ultrasonic velocity curves. Those features include the point where V_P starts to increase [7,11,13], the inflection point on velocity curve [17], or when V_P reaches the velocity in water [18]. To eliminate influence of air voids, some researchers used de-aired cement samples, and defined the setting point as the time when velocity starts to increase in de-aired samples [6,8,12,19]. However contradictory conclusions often result since some methods give very different setting time. It is still unclear how to determine the setting time based on P wave velocity measurement.

Although ultrasonic measurements obtained from de-aired cement samples show good correlation between P wave velocity and the setting time, using de-aired sample is unrealistic in field testing. On the other hand, quantitative study about effects of air voids on ultrasonic waves has been very limited. Recently, Kmack [20] experimentally investigated the effects of air voids on ultrasonic P wave propagation in fresh cement pastes by introducing various amount of air-entraining agent (AEA), 0–0.6% by weigh of cement. Kmack found that ultrasonic waves in air-entrained specimens showed significantly lower wave velocity and signal amplitude at early ages than the non-air-entrained specimens.

Shear waves have also been examined for monitoring setting and hardening of fresh cement pastes. Because shear waves have very low velocity and high attenuation in fluid cement paste, with the transmission setup, shear waves could only be detected a few hours after mixing. D'Angelo et al. [5] showed that shear waves are more

* Corresponding author.
E-mail address: jyzhu@mail.utexas.edu (J. Zhu).

0008-8846/$ – see front matter © 2011 Elsevier Ltd. All rights reserved.
doi:10.1016/j.cemconres.2011.04.005

sensitive to solid structure development than P waves, and the onset of shear waves is related to the cement thickening time. Thickening time is used in oilfield industry to describe the duration that a cement slurry remains in a fluid state and is capable of being pumped. It was also found that the development of shear wave energy is correlated with the volume fraction of connected solids in cement paste [21]. However the onset of S waves is affected by the sensitivity of equipment. Changing driving voltage, receiver gain or specimen size could affect the onset time of shear waves. Boumiz et al. [4] also believed that the onset of shear waves indicates percolation threshold. The shear wave velocity V_S and attenuation $\alpha_S(f)$ provide important information about the solid frame modulus and viscosity of cement pastes [4]. In most of studies using the transmission setup, shear waves were usually not observed until initial setting. To overcome this difficulty, the shear wave reflection method was proposed to monitor acoustic impedance change of cement paste at early ages, which relies on the solid microstructural development during setting and hardening [9,10,16,17,22]. The shear wave reflection method needs access to one test surface only, which makes it attractive for field testing. However, this setup measures the material properties on the surface only, which can be problematic because the surface of concrete typically has a higher porosity than the interior of concrete. Furthermore, the surface may set at a different time than the interior concrete. It has also been found that the property of the buffer material affects the setting time measurement [23].

In this study, the effects of air voids on ultrasonic wave velocity were investigated based on Biot's theory for poroelastic materials. In the experimental study, both the compressional and shear waves were monitored in cement pastes with two water/cement ratios (w/c = 0.4 and 0.5) and different air contents (0.1%–5.3%). The air voids were introduced by using air entraining admixtures (0, 0.01, 0.05, and 0.2% of cement weight). Experimental results indicated that existence of air voids in cement paste strongly affects the P wave velocity, but has little effect on the shear wave propagation.

2. Theory

2.1. Biot's theory

Although cement paste is usually regarded as a suspension at very beginning of the hydration, Harker and Temple have shown that a dense suspension with a large volume fraction of solid particles should be treated as a porous elastic material saturated with viscous fluid [24]. The propagation of elastic waves in a porous elastic solid saturated with a compressible viscous fluid has been treated by Biot [25,26]. An important finding of Biot theory is that two compressional waves (the fast and slow P waves) and one shear wave propagate in a fluid saturated porous solid. The fast wave exists in all frequency ranges, while the slow wave only exists in high frequency range. The critical frequency separating low and high frequency ranges depends on the fluid viscosity and pore size. At high frequencies, the effect of fluid viscosity is confined to a thin boundary layer near the solid/fluid interface [12], and the viscous skin depth $\delta = \sqrt{\eta/\rho_f\omega}$ is much smaller than the pore size. Here η is the viscosity of the pore fluid, ρ_f is the density of fluid, and ω is the angular frequency of wave. Sayer et al. [8,12] have shown that the high frequency Biot's theory applies to cement pastes at early ages since the pore size is large and viscosity of the fluid is low, while the low frequency Biot's theory applies to cement pastes at later ages. In de-aired cement pastes with weak solid frames, they reported that only the fast P wave was observed, which has a constant velocity (close to the water velocity) before setting. This result indicates that the fast P wave mainly propagates through the fluid phase; therefore it does not provide much useful information about the solid microstructure before initial setting.

In a weak frame medium and at high frequency limit, the fast and slow P wave velocities V_{P1} and V_{P2}, and shear wave velocity V_S are given by [27]

$$V_{P1,2}^2 = \frac{\Delta \pm \sqrt{\Delta^2 - 4(\rho_{11}\rho_{22} - \rho_{12}^2)(PR - Q^2)}}{2(\rho_{11}\rho_{22} - \rho_{12}^2)}, \tag{1}$$

$$V_S^2 = \frac{G}{(1-\phi)\rho_s + (1-1/\alpha)\phi\rho_f}, \tag{2}$$

where P, Q, and R are generalized elastic coefficients and are given as [12,27]

$$P = \frac{(1-\phi)(1-\phi-K/K_s)K_s + \phi K_s K/K_f}{1-\phi-K/K_s + \phi K_s/K_f} + \frac{4}{3}G, \tag{3}$$

$$Q = \frac{(1-\phi-K/K_s)\phi K_s}{1-\phi-K/K_s + \phi K_s/K_f}, \tag{4}$$

$$R = \frac{\phi^2 K_s}{1-\phi-K/K_s + \phi K_s/K_f}, \tag{5}$$

and

$$\Delta = P\rho_{22} + R\rho_{11} - 2Q\rho_{12}. \tag{6}$$

In these equations, K_f, K_s and K are the bulk moduli of the fluid, solid and frame. ϕ is the porosity, which is equals to the fluid volume fraction. The density terms ρ_{ij} are related to the solid density ρ_s and fluid density ρ_f by [12]

$$\rho_{11} + \rho_{22} = (1-\phi)\rho_s, \tag{7}$$

$$\rho_{22} + \rho_{12} = \phi\rho_f, \tag{8}$$

$$\rho_{12} = -(\alpha-1)\phi\rho_f. \tag{9}$$

Where α is the tortuosity and given as $\alpha = (1+\phi^{-1})/2$.

Fig. 1 shows the variation of V_{P1} and V_S as functions of shear modulus G of the solid frame, based on the equations shown above. For a cement pate with w/c = 0.4 and cement density of $\rho_s = 3180 kg/m^3$, the porosity is calculated as $\phi = 0.56$, and $\alpha = 1.39$. Other material parameters are chosen based on Ref. [12], and they are

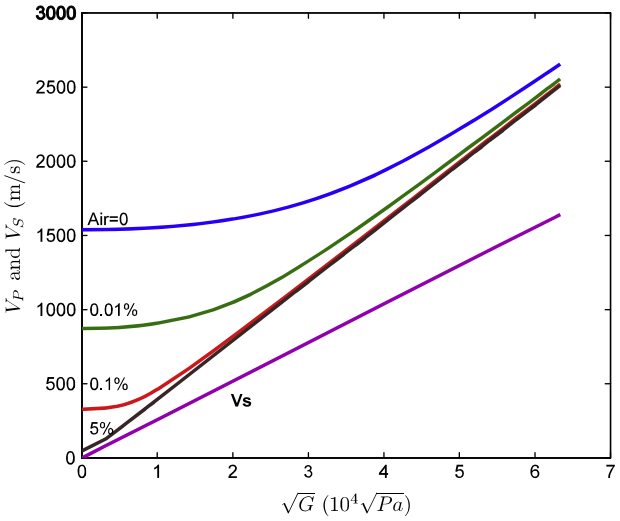

Fig. 1. Theoretical analysis of wave velocity variation with the solid frame shear modulus G in cement pastes with different air void contents (percentage of the fluid phase).

Poisson's ratio of the frame $\upsilon = 0.2$, and the bulk modulus of the solid and fluid phases $K_s = 50$GPa, and $K_f = 2.2$GPa. The calculation based on Biot's theory shows that the fast P wave velocity V_{P1} is close to the velocity in water (1500 m/s) when the solid frame is weak (K and G are small); while in the stiff frame limit, V_{P1} increases with the frame modulus G. This result agrees with experimental observations obtained in a de-aired cement paste. Based on this analysis, at early ages, the fast wave should mainly involve motion of the fluid phase of cement paste; but at late ages, it should involve motion of the solid frame of cement paste. Fig. 1 also shows that the shear wave velocity V_S is a linear function of $\sqrt{G}$, which indicates that the shear wave should involve motion of the solid frame only. Since only the fast P wave is usually measured, we simply use V_P to denote the fast P wave velocity thereafter in the paper.

2.2. Effects of air voids in the fluid phase

Following Keating's study [6], many researchers used de-aired cement pastes to study ultrasonic waves in early age cement pastes, and reached the conclusion that "*during the suspension period, ultrasonic velocity is not very sensitive to the growth of structure in the paste*" [19,28]. However, when a small amount of air bubbles, even less than 1%, were included in the cement paste, the P wave velocity will decrease dramatically, as observed by many researchers [6,13]. In this case, the P wave velocity V_P depends on the moduli of both the bubbly fluid and the solid frame, instead of the fluid phase only as in the de-aired case. Therefore, V_P will increase with the hydration process, and give information about the microstructural development of cement paste.

When a small amount of air bubbles present in cement paste, the bulk modulus of the fluid phase K_f should be modified to include the effect of air. Denote the bulk modulus of air as K_a, and the degree of saturation as S, then the volumetric percentage of air bubbles in the fluid phase is $1.0 - S$. The modified bulk modulus of the fluid phase is given as

$$\frac{1}{K_{fa}} = \frac{S}{K_f} + \frac{1-S}{K_a}. \tag{10}$$

For example, for fluid with 0.1% of air voids ($S = 0.999$), using $K_a = 1.4 \times 10^5$ Pa, the fluid modulus K_{fa} will decrease to 4.4% of the original value of K_f based on a calculation using Eq. (10). The corresponding velocity in water with air bubbles will drop to 311 m/s from 1500 m/s in water without air. Replacing K_f with K_{fa} in Eq. (1), the P wave velocity in cement paste containing air bubbles can be calculated. Fig. 1 shows the variation of V_P and V_s with solid frame shear modulus G, for different air contents (percentage of the fluid phase). It can be seen that the P wave velocity drops dramatically when air bubbles present in the fluid phase. When the air content increases from 0 to 0.01%, 0.1% and 5% (corresponding to cement paste air content 0%, 0.0056%, 0.056% and 2.8%), the P wave velocities in very weak frame media become 1500, 843, 316 and 46 m/s. The P wave velocity can be lower than the velocity in air (340 m/s) when air content in fluid is larger than 1%. The analysis also shows that the trend of velocity drop with air content is not linear. V_P is very sensitive to small amount of air bubbles in fluid, but becomes insensitive when air content is larger than 5%. These phenomena have also been observed in experiments by the authors and other researchers [20]. The analysis result in Fig. 1 also shows that the shear wave velocity is still a linear function of $\sqrt{G}$, and should not be affected by presence of air voids.

3. Experimental study

3.1. Materials and sample preparation

The cement used in this investigation was Type I/II ordinary Portland cement with a Blaine fineness of 382 m^2/kg and chemical composition of 21% SiO_2, 5% Al_2O_3, 3.1% Fe_2O_3, 1.1% MgO, 2.9% SO3, and 2.9% LOI.

Ten cement paste mixtures were prepared according to the proportions shown in Table 1. The mixture compositions were selected to span a wide variety of air contents and two water/cement ratios (0.4 and 0.5). For each water/cement ratio, five mixtures with different air contents were prepared. Air voids were introduced into the pastes by using air entraining agent (AEA) with four different doses (0, 0.01, 0.05, and 0.2% by cement weight). The air entraining agent (Sika air) is an aqueous solution of organic materials satisfying the requirement of ASTM C-260 [29]. One de-aired sample was prepared by storing a non-air-entrained mixture in a low pressure chamber for 30 minutes.

3.2. Ultrasonic test setup

Fig. 2 illustrates the test setup for monitoring ultrasonic wave propagation through the cement paste samples. The test setup includes a U shape rubber container and a cover, four pieces of 5 mm thick Plexiglas plates, a pair of ultrasonic transducers, and their housing. Two inner Plexiglas plates and the rubber form a container. A layer of soft foam was inserted between the plates and the rubber to avoid direct bypass of ultrasonic waves through the test setup. A rubber cover was designed to prevent water evaporation from sample surface so that dry shrinkages can be minimized. A pair of ultrasonic transducers contact the outside surface of the Plexiglas plates through ultrasonic couplant, as shown in Fig. 2. The outer Plexiglas plates are used to press the transducers to maintain good coupling. In this study, three types of ultrasonic transducers were used to generate P waves and S waves at different center frequencies. Panametrics V101 (P wave) and V151 (S wave) are broad band ultrasonic transducers with nominal center frequency of 500 kHz. A Panametrics 5077PR pulser–receiver was used to drive the 500 kHz transducers. The 5077PR has square wave excitation with tunable pulse width and voltage. In this study, the driving voltage was 100 V, with a pulse width 1 μs to match the 500 kHz transducer. The shear wave transducer tests were used to check the accuracy of shear wave velocity obtained from the P wave transducer tests. The Pundit UPV transducers are narrow band transducers with center frequency around 50 kHz. A Pundit 7 ultrasonic pulse velocity unit was used to drive and receive the 50 kHz transducers, with driving voltage of 1000 V. Setups for these three types of transducers were similar, but with different sample thickness L. The sample thickness for the 500 kHz test setup was 25 mm, and for the 50 kHz test setup was 100 mm. These lengths were chosen to make sure that there is at least one wavelength distance between the transducers. In the P wave

Table 1
Summary of mix proportions, air void system parameters and setting times.

Specimens	Transducer type and frequency (kHz)	Mix proportion		Parameters related to the air void system			Time of set	
		w/c	AEA (% of cement)	A [%]	N	l [μm]	Initial [h]	Final [h]
1[a]	50,500 P	0.4	0	0.09	16	182.3	4.3	5.2
2	50,500 PS[b]		0	0.21	71	133.3	4.4	5.3
3	50,500 P		0.01	0.79	309	124.3	4.9	5.7
4	50,500 PS[b]		0.05	1.59	704	117.7	4.6	5.55
5	50,500 P		0.2	2.28	1962	87.2	4.7	5.5
6[a]	50,500 P	0.5	0	–	–	–	5	6.5
7	50,500 PS[b]		0	0.56	232	124.2	5.2	6.6
8	50,500 P		0.01	1.12	488	118.9	5.6	6.9
9	50,500 PS[b]		0.05	–	–	–	5.3	6.75
10	50,500 P		0.2	5.30	2097	127.35	5.4	6.8

[c]Cement paste thickness is 25 mm for 500 kHz tests, and 100 mm for 50 kHz tests.
[a] De-aired through the vacuum process.
[b] 500 PS indicates that the mixture was monitored with 500 kHz P wave and S wave transducers.

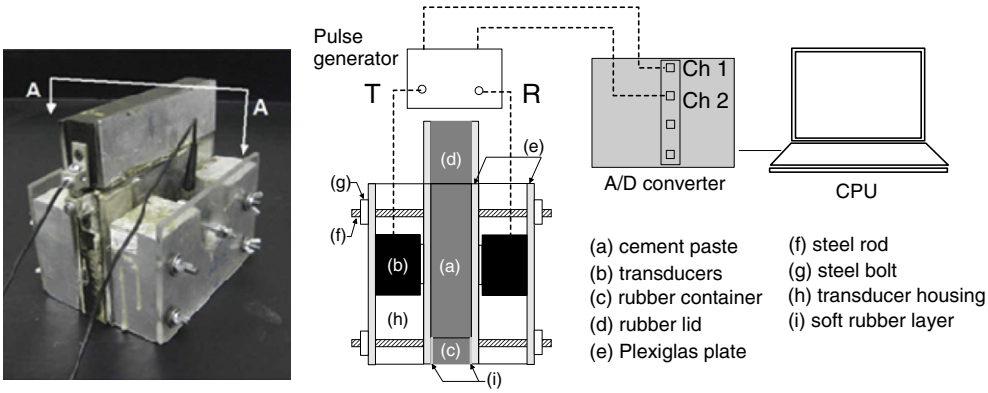

Fig. 2. Test setup and data acquisition system of ultrasonic measurement.

tests, petroleum jelly was used as a couplant to ensure good contact between transducers and Plexiglas plates throughout the test. In the shear wave tests, high viscosity shear wave couplant made by Sonotech was used to ensure effective shear wave transmission. Output signals from the pulser–receiver were digitized by an National Instruments high speed digitizer. The sampling frequency was 10 Ms/s for the 50 kHz transducers, and 20 Ms/s for the 500 kHz transducers. The number of samples was 10,000 for 500 kHz, and 6000 for 50 kHz transducers, which give signal length of 500 μs and 600 μs, respectively. For each cement paste mixture, the 500 kHz and 50 kHz P wave transducer tests were running simultaneously.

Because the amplitude of ultrasonic signals changes by several orders of magnitude during the cement hydration process, vertical ranges of the digitizers were programmed to automatically adjust to the amplitude of received signals. This can ensure best vertical resolution of signals throughout cement hydration process from suspension state (low energy transmission) to solid state (much higher energy transmission). Furthermore, to increase the signal to noise ratio, 150 signals were averaged. The program saved averaged signals every 5 minutes. The entire process of data acquisition and recording was automatically controlled by a Labview® program developed by the authors. Measurement of ultrasound continued for approximately 20 hours after mixing cement pastes.

3.3. Vicat-needle test

Along with ultrasonic tests, the Vicat-needle tests were carried out in accordance with ASTM C191 [1] to measure the setting time of the specimens. The cement paste specimen was kept in a sealed container with relative humidity consistently maintained higher than 50% excepting during test. Test results are shown in Table 1.

3.4. Characterization of the air void system

Air contents were measured on hardened cement pastes after the ultrasonic monitoring. The linear transverse method described in ASTM C457 [30] was used in conjunction with a digital image processing technique to determine characteristics of the air-void system. Sections of samples were obtained by sawing the hardened cement paste specimens along the plane parallel to the ultrasonic test surfaces. The section surfaces were carefully prepared according to ASTM C457 [30]. The sample section was polished and dyed using water-based black ink. After the section was completely dry, pores of the air void were then filled with white powder (calcium carbonate power) to improve contrast between the voids and paste. Finally, the sample section was digitized using a digital scanner for further image processing. One image was obtained for each specimen. The resolution of digital images is 1200 dpi, i.e., one pixel represents about a 20×20μm square.

4. Air voids and setting time results

4.1. The air void system of specimens

Fig. 3 shows black-and-white section images of cement paste samples with different w/c and AEA doses. The white regions in images represent air voids, and the black regions are for the portion of cement paste. It can be seen that the air void content of cement pastes varies as a function of the amount of AEA and w/c.

Air voids of cement paste specimens were characterized by several geometric factors described in ASTM C 457 [30]: (i) air content A, (ii) paste content p, (iii) the number of air-voids, and (iv) average chord length $\bar{l}$. The geometric factors are defined as follows:

$$A = \frac{A_a}{A_t} \times 100[\%] \tag{11}$$

$$p = \frac{A_p}{A_t} \times 100[\%](\text{or } 100-A\ [\%]) \tag{12}$$

$$\bar{l} = \frac{1}{N}\sum_{i=1}^{N} \phi_i \tag{13}$$

where A_a and A_p are the area of white and black regions, respectively; A_t is $A_a + A_p$, ϕ is the radius of air voids, and N is the total number of air voids in the section. In this study, the geometric factors were calculated by a MATLAB® code using the image processing toolbox, and the results are summarized in Table 1. The image analysis shows that the cement pastes investigated in this study contain 0.1%–5.3% air voids. For the same dosage of AEA, pastes with 0.5 w/c have higher air content than the 0.4 w/c pastes. The average size of air voids is about 125 μm.

4.2. Vicat results

The initial and final setting times were determined by the Vicat needle test for all specimens, and are summarized in Table 1. Results show that the non-air-entrained specimens have earlier setting times than the air-entrained specimens. However, the setting time does not increase with the AEA amount linearly. For example, the pastes with 0.01% AEA for both 0.4 and 0.5 w/c set later than the pastes with 0.2% AEA.

5. Ultrasonic test results

5.1. B-scan images of ultrasonic waves

Images are formed by stacking up a series of normalized ultrasonic wave signals recorded at different ages, with the x-axis representing the time of signals (unit: microseconds), and y-axis for ages of cement

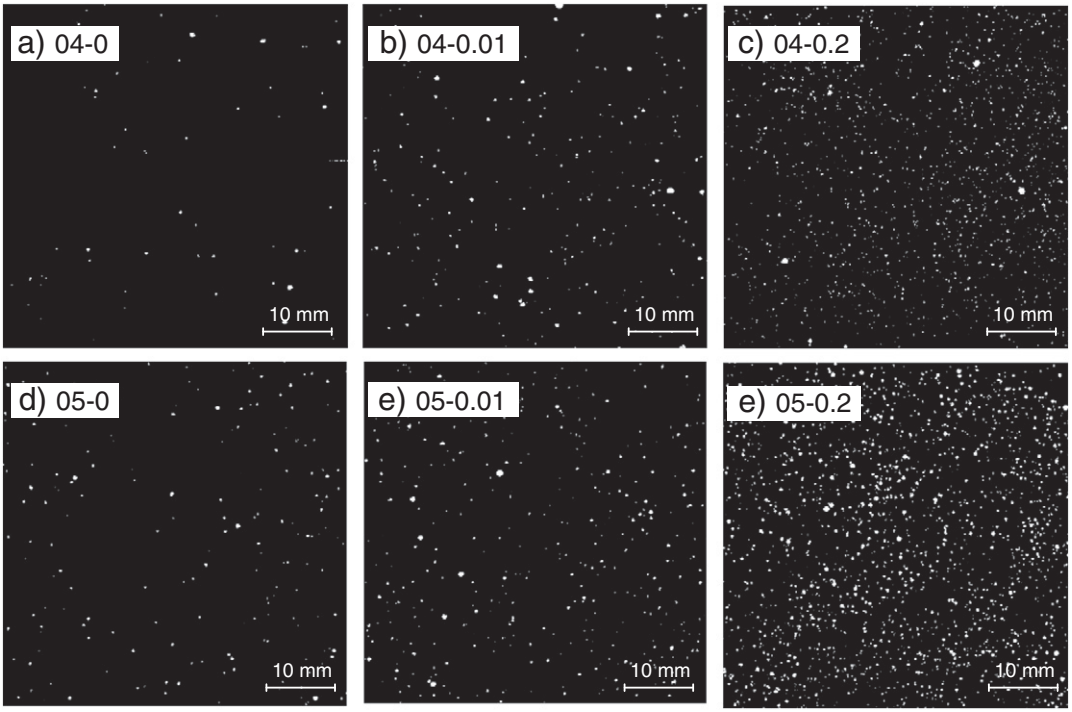

Fig. 3. Typical sectional images of specimens with various mix proportions: (a) w/c = 0.4, and AE = 0%; (b) w/c = 0.4, and AEA 0.01%; (c) w/c = 0.4, and AEA 0.05%; (d) w/c = 0.5, and AEA 0%; (e) w/c = 0.5, and AEA 0.01%; and (f) w/c = 0.5, and AEA 0.2%.

pastes (unit: hours). Brightness of the grayscale images represents the amplitude of signals, with bright color for positive amplitudes, and dark color for negative amplitudes. Due to the similarity between the obtained images (time vs. age) and the B-scan images (time vs. scanning distance) used in ultrasonic NDT field, we use the term 'B-scan' to name the ultrasonic signal images in this study. Because the amplitudes of ultrasonic wave signals at later ages are several orders higher than that at early ages, each signal was first normalized by its maximum amplitude, so that all signals have the same normalized peak amplitude 1.0. In Fig. 4(a)–(d), to distinguish shear waves, the color scale is set as [−0.1, 0.1]. In Fig. 4(e) and (f), the color scale is set as [−1, 1].

5.1.1. 500 kHz P wave transducers

Fig. 4 shows a series of B-scan images of ultrasonic wave signals through cement pastes using the 500 kHz P wave transducers. The B-scan images are effective to identify different wave modes propagating through the cement pastes, which might be otherwise difficult to identify from a single waveform. In Fig. 4, images (a), (c), and (e) in the left column are for specimens with w/c = 0.4, and images (b), (d), and (f) in the right column are for specimens with w/c = 0.5. Images in the first, second and third rows are from the de-aired, no AEA, and 0.2% AEA samples, respectively. B-scan images corresponding to the specimens with AEA = 0.01 and 0.05% are not presented; however, characteristics of the wave propagation in these samples are similar to the samples with 0.2% AEA.

The images for de-aired specimens (Fig. 4(a) and (b)) show clear and strong P wave arrivals from very early ages, and the arrival time stays constant in the first 2 hours. During the 20 hours tests, the P wave have relative constant pulse width (or frequency), which is shown as constant width of the bright color regions. Multiple reflections of P waves are also clearly observed, which resemble the first P wave pulses but arrive at later time. In addition to P waves, shear waves are also observed, which have much lower amplitude comparing to the P waves. In images (a)–(d), the color scales are set as [−0.1, 0.1] to distinguish weak shear waves from dominant P waves. Several reflections of shear waves are also shown in these images. With the increase of cement ages, the arrival times of P and S waves decrease.

Fig. 4(c) and (d) show B-scan images for non-air-entrained cement pastes with w/c of 0.4 and 0.5. Small amount of air bubbles were entrapped in cement pastes during mixing. Air void analysis results (Table 1) show that the air contents in these two mixtures are 0.21% and 0.56%, respectively. Compared to the de-aired cases, the B-scan images for the non-AEA mixtures show several different features. First, the P wave arrival times at early ages (<3 hours) are much later than in the de-aired cases. Second, the P wave becomes dispersive at early ages, which is shown as wider pulse duration than in the late ages. Due to high attenuation at early ages, only the first P wave reflection is observed. Third, an interesting feature unique to the 0% AEA case is the high frequency waves that appear before the P wave arrival time. Spectral analysis shows that the resonant frequencies of these signals are around 600 kHz. This phenomenon was also observed by Sayers and Dahlin [12] in a mixture containing 2% $CaCl_2$, and by Kmack [20] in non-AEA cement pastes. Sayers explained that this high frequency wave was caused by resonant vibration of air bubbles in cement pastes. It is also seen that these air bubble resonance waves exist only when the cement pastes are still fresh, which corresponds to about 2.5 hours for w/c = 0.4 and 4.0 hours for w/c = 0.5 pastes in this study. Further analysis indicates the resonant wave has a velocity close to 1500 m/s, which agrees with previous study [12,20].

Fig. 4(e) and (f) show B-scan images for ultrasonic signals in cement pastes containing 0.2% AEA, with color scale of [−1.0, 1.0]. Overall the images are similar to the images in Fig. 4(c) and (d), but the early age high frequency waves are not present in this case. The P wave arrival time starts from 200 μs at early ages, and then gradually decreases with the age of cement paste. In the normalized images, the relative amplitudes of shear wave pulses are more prominent than in the low air content cases. This result indicates that air voids attenuate

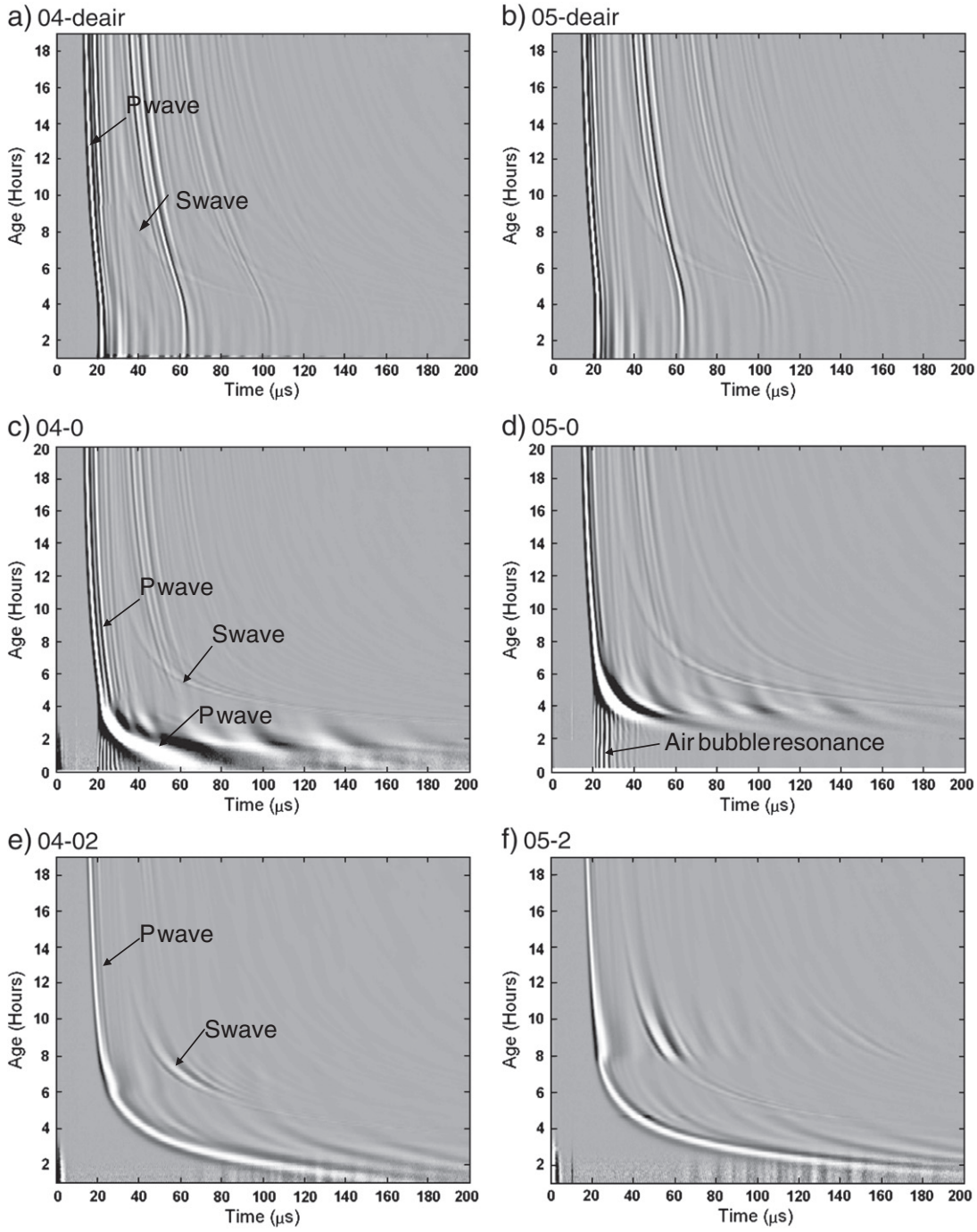

Fig. 4. B-scan images of normalized ultrasonic wave signals obtained from cement mixtures using the 500 kHz P wave transducers: (a) w/c = 0.4, de-aired, and AE = 0%; (b) w/c = 0.5, de-aired, and AE = 0%; (c) w/c = 0.4, and AE = 0%; (d) w/c = 0.5, and AE = 0%; (e) w/c = 0.4, and AE = 0.2%; and (f) w/c = 0.5, and AE = 0.2%. To distinguish shear waves, the color scale in (a)–(d) is set as [−0.1, 0.1]. The color scale for images (e)–(f) is [−1.0 1.0].

P waves more than S waves. Therefore, the signal amplitude ratio between S and P waves is high. Because the signals were obtained using the 500 kHz P wave transducers, the signals were still dominated by P waves.

The normalized time domain ultrasonic signals at 2 and 8 hours for cement pastes of w/c = 0.4 are shown in Fig. 5. At 2 hours, the P wave arrival time for 0.2% AEA specimen is much later than in the non-AEA and de-aired cases. The signal is very noisy and has low amplitude. Actually, the raw signal before normalization for the de-aired paste is seven orders higher than that in the 0.2% AEA paste. At this age, shear waves were not observed. At 8 hours (after final setting), both P and S waves were observed in the AEA = 0.2% case. In the other two cases, the relative amplitude of S waves with respect to the P waves is too small to be identified from a single signal. However, with the aid of B-scan images, it becomes easy to identify the S waves.

5.1.2. 500 kHz S wave transducers

Fig. 6 shows the B-scan image obtained from a cement paste with 0.4 w/c and 0% AEA, using the shear wave transducers. To clearly show the separation of S waves from P waves, only signals in the first 5 hours are shown. Compared to Fig. 4(c), the shear wave components in Fig. 6 are much stronger and clearer, and shear waves were

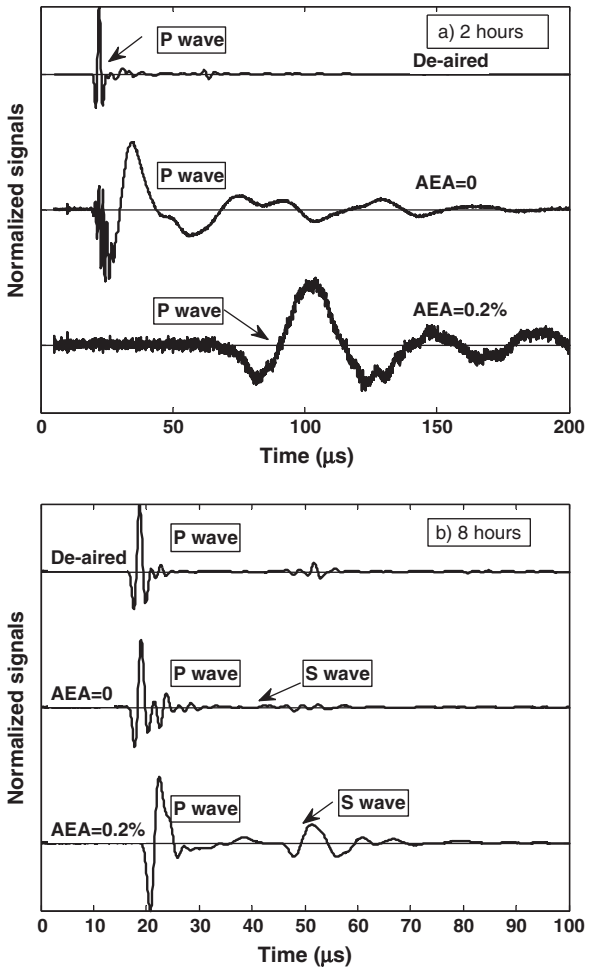

Fig. 5. Time domain ultrasonic signals at 2 and 8 hours for three cement pastes of w/c = 0.4.

observed even in the first hour after mixing. A comparison of velocity measurement using the P and S wave transducers are shown in Section 5.2.

5.1.3. 50 kHz P wave transducers

Fig. 7 shows a B-scan image of ultrasonic signals obtained by the 50 kHz UPV transducers on a cement paste with 0.4 w/c and 0% AEA. Because the transducers have a very narrow band and high impedance, there is a long signal ringing following the first P wave arrival. Compared to Fig. 4(c), the P wave arrival time show a similar trend with age. However, the high frequency waves at very early ages are not present in the 50 kHz image. According to Sayers [12] theory, that phenomenon is caused by air bubble resonance at high frequencies. The 50 kHz transducers are not able to excite the high frequency vibration. Shear waves are visible from 4 to 6 hours, and then overshadowed by ringing P wave signals.

5.2. Ultrasonic wave velocity

5.2.1. P and S wave velocity—500 kHz

The arrival times of P waves are usually determined by detecting the first signal point that exceeds a predetermined threshold. However, this method does not apply to shear wave arrival determination. In addition, the threshold method may give erroneous results on noisy signals, especially at early ages. In this study, we used a digitizing tool to directly obtain S wave arrival times from B-scan images. The velocity was calculated by dividing the wave path L over the travel time of waves through specimens $V = L/t$. The actual wave travel time t through cement pastes was determined by subtracting the time through the Plexiglas and couplants t_0 from the measured P or S wave arrival time. Fig. 8 shows the P and S wave velocities measured from all cement pastes using the 500 kHz P wave transducers. Velocities measured with the 500 kHz S wave transducers are shown in Fig. 9. For comparison, the results from P wave transducers are also shown. It can be seen that these two setups give very similar results. The P wave transducer setup gives a slightly higher P wave velocity because a higher P wave amplitude tends to give an earlier arrival times for a specified threshold value.

The effect of air voids on P wave velocities are clearly observed in Fig. 8. At early ages, with the increase of AEA dosages, the P wave velocities decrease dramatically, from 1500 m/s in the de-aired sample to about 200 m/s in air-entrained specimens. For w/c = 0.4, at late ages, non-AEA specimens show similar P wave velocities, and the air-entrained specimens have slightly lower velocities. For pastes with water/cement of 0.5, the air-entrained specimens show more decrease of V_P at late ages than in the 0.4 w/c specimens. The overall

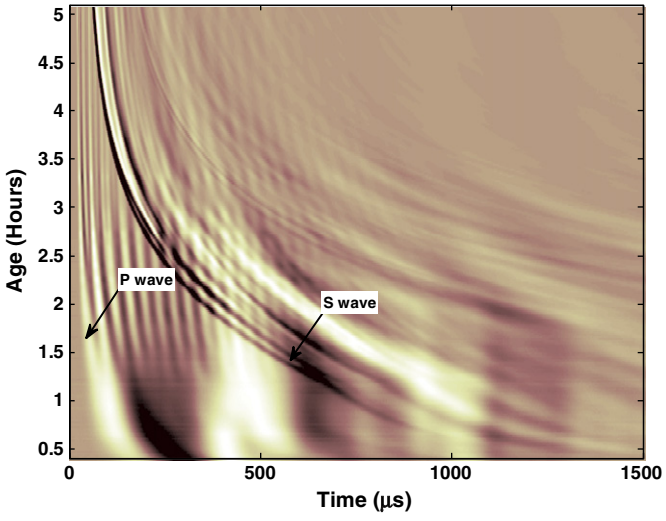

Fig. 6. Ultrasonic B-scan images obtained using the 500 kHz shear wave transducers from the cement paste of w/c = 0.4, and AE = 0%.

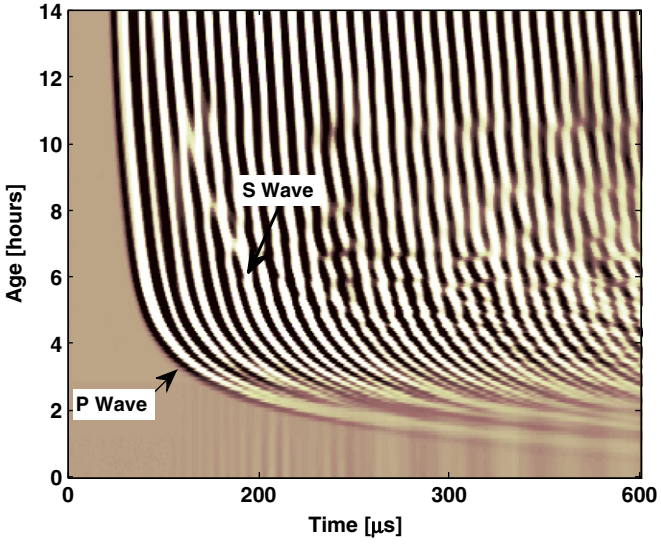

Fig. 7. B-scan image of ultrasonic wave signals obtained using the 50 kHz P wave transducers from a cement paste of w/c = 0.4, AEA = 0%.

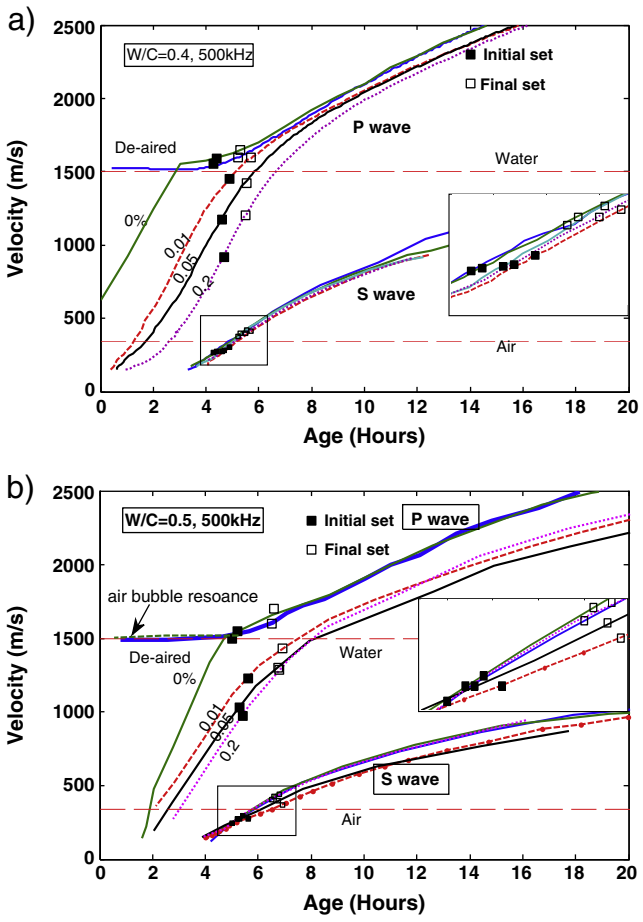

Fig. 8. Ultrasonic wave velocity measured from ten cement paste specimens using 500 kHz P wave transducers: (a) w/c = 0.4, and (b) w/c = 0.5. Initial and final setting times are marked on curves. Numbers in the figure represent AEA dose. The zoomed early age shear wave curves are also shown.

trend of P wave curves indicates that the air voids strongly affect P wave velocity at early ages, but have relatively little effect at late ages. On the other hand, presence of air voids has little effect on S wave velocity, especially in the 0.4 w/c cases. For w/c = 0.5 specimens, the S wave velocity curves show some difference for various air contents. However the S wave velocity differences at early ages are still smaller than in the P wave velocity data.

Setting times for all mixtures are also marked on Fig. 8 velocity curves. As seen in the figure, although the setting times for all cement pastes are very close (differ by 0.5 hour), the P wave velocity corresponding to the initial setting time is different for each cement paste. In the de-aired and non-air-entrained cement pastes, the initial setting times correspond to the points where V_P starts to increase. However, for all air-entrained cement pastes, the initial setting times do not correspond to certain features on the P wave velocity curve, such as start increasing point, inflection point, or water velocity point [7,11,13,17,18]. However, the shear wave velocities at the initial setting times are almost the same for all specimens. More detailed discussion is given in Section 6.

Fig. 10 plots the measured V_P against V_S for all w/c = 0.4 cement pastes with different air contents. Since V_s reflects modulus development of the solid frame (Eq. 2), Fig. 10 represents the P wave variation with the solid frame stiffness. Comparing Fig. 10 with the theoretical analysis results in Fig. 1, it can be noticed that the experimental results show a similar trend as predicted as the Biot's theory.

5.2.2. P and S wave velocity—50 kHz

Wave velocities measured by the 50 kHz transducers for w/c = 0.4 cement pastes are shown in Fig. 11. For comparison, the P wave velocity measured with the 500 kHz transducers is also shown for mixture AEA = 0.2%. Overall, the conclusions obtained from the 500 kHz tests also apply to the 50 kHz tests. For all pastes containing air voids, the P wave velocities start at a very low value and gradually increase with ages. The de-aired and non-air-entrained pastes show almost the same velocity after initial setting.

5.3. Correlation between wave velocities and setting times

Initial and final setting times determined by the Vicat needle test for all specimens are summarized in Table 1. The ten specimens cover different air void contents from 0.2% to 5.5%. The wave velocities corresponding to the setting times are also marked in Fig. 8. Fig. 11 plots the P and S wave velocities corresponding to the initial and final setting times versus the air contents. As shown in the plot, for air content less than 2%, V_P at the setting time decreases with increasing air content in cement pastes. For the de-aired specimens, V_P at the initial setting time is around 1500 m/s; however, as the air content increases to 2%, V_P at the

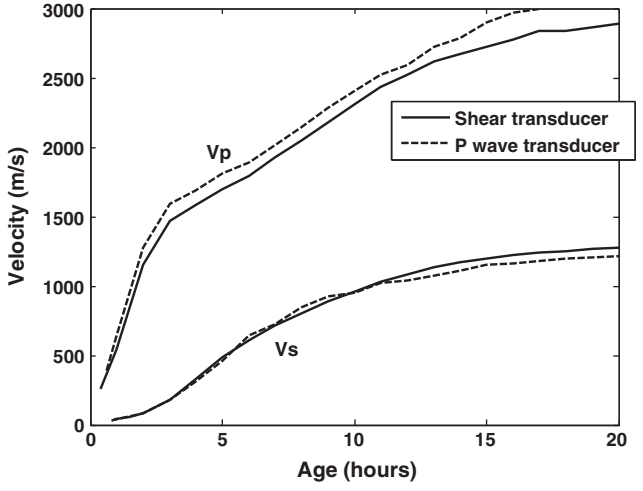

Fig. 9. Comparison of measured wave velocities using the 500 kHz P wave and S wave transducers.

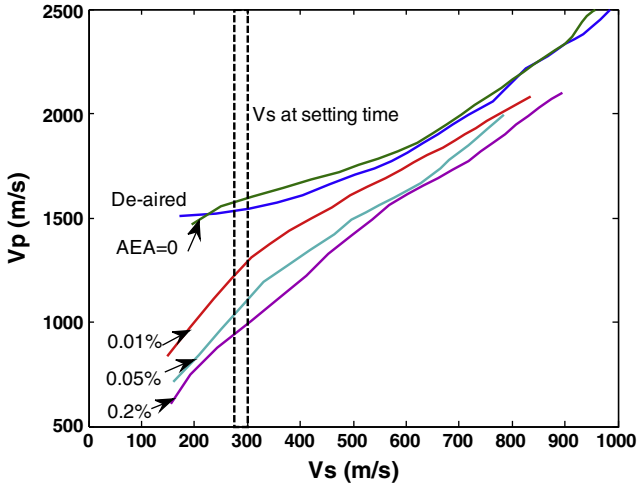

Fig. 10. Measured ultrasonic P wave velocity vs. S wave velocity for cement pastes (w/c = 0.4) with different air contents. The dash lines mark the range of shear wave velocity at initial setting times.

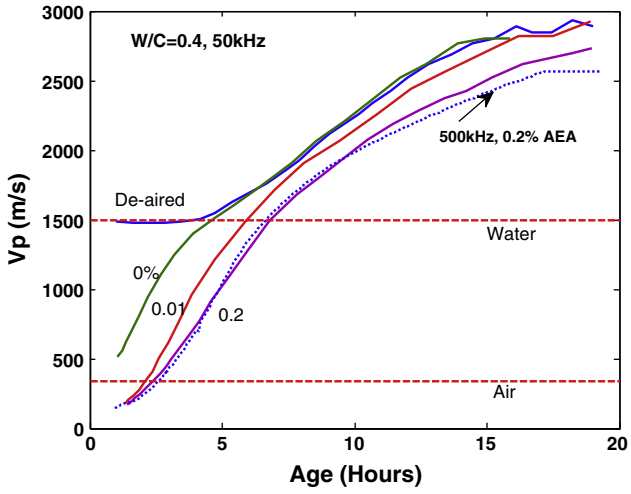

Fig. 11. Measured ultrasonic P wave velocity for w/c = 0.4 cement mixtures using the 50 kHz transducers. For comparison, the 500 kHz test result for AEA = 0.2% is also shown.

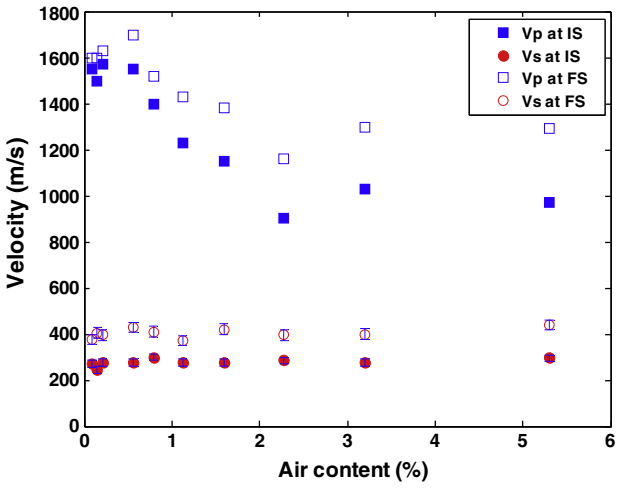

Fig. 12. Ultrasonic P and S wave velocities at initial and final setting times for all cement paste specimens with different air void contents (w/c = 0.4 and 0.5). Ultrasonic P and S wave velocities were measured with the 500 kHz P wave transducers. The initial setting times were determined from the Vicat test. Error bars are shown for S wave data.

initial setting time decreases to about 900 m/s. Further increasing air content from 2% to 5% has relatively little effect on V_P.

Unlike the P wave velocity, the S wave velocity V_S at setting times are not sensitive to air content changes. Although the specimens in this study have different mix proportions and setting times, the shear wave velocity V_S at the initial setting times are approximately in the range of 270–300 m/s for all cement pastes, which covers 0.1% to 5.5% air content. The shear wave velocity V_S at the final setting times are around 400 m/s. This experimental finding verifies the conclusions in the theory section: the shear wave velocity V_S is related to the solid frame stiffness G, and the relationship between them should not be affected by air voids in cement pastes.

6. Discussion

Although many studies have tried to correlate the ultrasonic P wave velocity with setting times of cement, there was still no clear answer to this question. According to Biot's theory, in the early age de-aired cement pastes, the P wave propagation mainly involves motion in the fluid phase. In this case, the P wave velocity is close to the velocity of the fluid phase, and it is not related to the solid frame microstructural development before setting time. For air-entrained cement pastes, however, from very beginning of the cement hydration, the P wave propagation involves motion in both the fluid phase and the solid frame, which is shown as continuous increase of P wave velocity with ages (Figs. 8, 9 and 11) and the solid frame stiffness (Figs. 1 and 10). This conclusion provides the base for using P waves to monitor setting and hardening process of cement pastes.

However, theoretical analysis and experimental results presented in this study show that the P wave velocity is strongly affected by the air void contents in cement pastes at early ages, especially for small amount of air voids. This effect decreases at high level of air content. Fig. 1 predicts that the effect of air voids on V_P becomes saturated when the air void content (by volume of fluid phase) is large than 5% (2.8% by cement paste volume). It has been verified by the experimental results in Fig. 12.

Shear wave propagation mainly involves the solid frame only, and the S wave velocity is directly related to the shear modulus of solid frame. The Vicat test measures the shear resistance of cement pastes. Therefore, it is not a surprise to see strong correlation between the S wave velocity and setting time determined by the Vicat test. Compared to P waves, the S waves are less affected by air voids and fluid phase property. However, the shear wave velocity measurement did not receive the same level of attention as the P waves. One possible reason is that the high attenuation in cement pastes prevents detection of shear waves at early ages [4,5]; therefore the onset of shear waves was used as an indication of initial setting. In this study, using the shear wave transducer setup, combined with B-scan images, the shear waves can be detected as early as 30 minutes after mixing. The shear wave method shows great potential for monitoring setting and hardening process of cementitious materials.

7. Conclusions

This paper presents a study to investigate air void effects on ultrasonic wave propagation in fresh cement pastes. Based on experimental study and theoretical analysis, the following conclusions are obtained.

1) The ultrasonic P wave velocity is strongly affected by air voids in early age cement pastes. One percent of air voids in fresh cement paste will reduce the P wave velocity from 1500 m/s to about 200 m/s. When air content is higher than 2%, V_P becomes less sensitive to air content changes.
2) In non-de-aired, non-air-entrained cement pastes, in addition to P and S waves propagating in the solid phase, there is another type of wave caused by air voids resonance in the fluid phase, which propagates at 1500 m/s (water velocity). This type of wave is only observed in pastes with small amount of air voids, and when the input frequency is close to the resonant frequency, which is around 600 kHz in this study.
3) There is no clear relationship between the P wave velocity and initial setting time by the Vicat test. In de-aired or low air content samples, the initial setting occurs when V_P starts to increase. However, in cement pastes with air voids, the initial setting time does not correspond to certain features on the P wave velocity curve.
4) The shear wave velocity reflects the solid frame microstructural development in fresh cement pastes. Therefore, V_S is less affected by air voids than V_P. Experimental results show that V_S at setting times has relatively constant values for all cement mixtures, with different w/c and air contents. With 500 kHz ultrasonic transducers, the measured V_S at initial setting times are 270–300 m/s, and at final setting times are around 400 m/s. This study shows the potential of using shear wave velocity to monitor setting process of cement and concrete.

5) Ultrasonic B-scan images illustrate the ultrasonic wave variation during cement hydration process. With the aid of B-scan images, it is easy to identify different wave modes propagating through the cement pastes, and determine the arrival time of each wave mode, which could be difficult to identify from a single waveform signal.

References

[1] ASTM C191, Standard test methods for time of setting of hydraulic cement by Vicat needle, American Society for Testing and Materials, Pennsylvania.
[2] L. Struble, H. Zhang, G.-K. Sun, W.-G. Lei, Oscillatory shear behavior of portland cement paste during early hydration, Concrete Science and Engineering 2 (9) (2000) 141–149.
[3] G. Sant, C.F. Ferraris, J. Weiss, Rheological properties of cement pastes: a discussion of structure formation and mechanical property development, Cement and Concrete Research 38 (11) (2008) 1286–1296.
[4] A. Boumiz, C. Vernet, F.C. Tenoudji, Mechanical properties of cement pastes and mortars at early ages: evolution with time and degree of hydration, Advanced Cement Based Materials 3 (3–4) (1996) 94–106.
[5] R. D'Angelo, T.J. Plona, L.M. Schwartz, P. Coveney, Ultrasonic measurements on hydrating cement slurries: onset of shear wave propagation, Advanced Cement Based Materials 2 (1) (1995) 8–14.
[6] J. Keating, D. Hannant, A. Hibbert, Comparison of shear modulus and pulse velocity techniques to measure the buildup of structure in fresh cement pastes used in oil-well cementing, Cement and Concrete Research 19 (4) (1989) 554–566.
[7] H. Reinhardt, C. Grosse, Continuous monitoring of setting and hardening of mortar and concrete, Construction and Building Materials 18 (3) (2004) 145–154.
[8] C.M. Sayers, R.L. Grenfell, Ultrasonic propagation through hydrating cements, Ultrasonics 31 (3) (1993) 147–153.
[9] Z. Sun, T. Voigt, S.P. Shah, Rheometric and ultrasonic investigations of viscoelastic properties of fresh portland cement pastes, Cement and Concrete Research 36 (2) (2006) 278–287.
[10] T. Voigt, G. Ye, Z. Sun, S.P. Shah, K. van Breugel, Early age microstructure of portland cement mortar investigated by ultrasonic shear waves and numerical simulation, Cement and Concrete Research 35 (5) (2005) 858–866.
[11] T. Chotard, N. Gimet-Breart, A. Smith, D. Fargeot, J.P. Bonnet, C. Gault, Application of ultrasonic testing to describe the hydration of calcium aluminate cement at the early age, Cement and Concrete Research 31 (3) (2001) 405–412.
[12] C. Sayers, A. Dahlin, Propagation of ultrasound through hydrating cement pastes at early times, Advanced Cement Based Materials 1 (1) (1993) 12–21.
[13] G. Ye, K. Van Breugel, A. Fraaij, Experimental study and numerical simulation on the formation of microstructure in cementitious materials at early age, Cement and Concrete Research 33 (2) (2003) 233–239.
[14] H. Lee, K. Lee, Y. Kim, H. Yim, D. Bae, Ultrasonic in-situ monitoring of setting process of high-performance concrete, Cement and Concrete Research 34 (4) (2004) 631–640.
[15] L. Qin, Z. Li, Monitoring of cement hydration using embedded piezoelectric transducers, Smart Materials and Structures 17 (5) (2008).
[16] J. Rapoport, J. Popovics, S. Kolluru, S. Shah, Using ultrasound to monitor stiffening process of concrete with admixtures, ACI Materials Journal 97 (6).
[17] T. Voigt, C. Grosse, Z. Sun, S. Shah, H. Reinhardt, Comparison of ultrasonic wave transmission and reflection measurements with p-and s-waves on early age mortar and concrete, Materials and Structures 38 (8) (2005) 729–738.
[18] G. Trtnik, G. Turk, F. Kavcic, V.B. Bosiljkov, Possibilities of using the ultrasonic wave transmission method to estimate initial setting time of cement paste, Cement and Concrete Research 38 (11) (2008) 1336–1342.
[19] J. Keating, D. Hannant, A. Hibbert, Correlation between cube strength, ultrasonic pulse velocity, and volume change for oil-well cement slurries, Cement and Concrete Research 19 (5) (1989) 715–726.
[20] R. M. Kmack, Characterization of air voids in fresh cement paste through ultrasonic nondestructive testing, Master's thesis, Georgia Institute of Technology (2008).
[21] D. Bentz, P. Coveney, E. Garboczi, M. Kleyn, P. Stutzman, Cellular automaton simulations of cement hydration and microstructure development, Modelling and Simulation in Materials Science and Engineering 2 (4) (1994) 783–808.
[22] K. Subramaniam, J. Lee, Ultrasonic assessment of early-age changes in the material properties of cementitious materials, Materials and Structures 40 (3) (2007) 301–309.
[23] C. Chung, J. Popovics, L. Struble, Early age stiffening of cement paste using ultrasonic wave reflection, ACI-SP: transition from fluid to solid: re-examining the behavior of concrete at early ages, 2009.
[24] A. Harker, J. Temple, Velocity and attenuation of ultrasound in suspensions of particles in fluids, Journal of Physics D: Applied Physics 21 (11) (1988) 1576–1588.
[25] M.A. Biot, theory of propagation of elastic waves in a fluid-saturated porous solid. I. Low-frequency range, The Journal of the Acoustical Society of America 28 (2) (1956) 168–178.
[26] M.A. Biot, Theory of propagation of elastic waves in a fluid-saturated porous solid. II. Higher frequency range, The Journal of the Acoustical Society of America 28 (2) (1956) 179–191.
[27] D.L. Johnson, T.J. Plona, Acoustic slow waves and the consolidation transition, The Journal of the Acoustical Society of America 72 (2) (1982) 556–565.
[28] G. Ye, P. Lura, K. van Breugel, A.L.A. Fraaij, Study on the development of the microstructure in cement-based materials by means of numerical simulation and ultrasonic pulse velocity measurement, Cement and Concrete Composites 26 (2004) 491–497.
[29] ASTM C260, Standard specification for air-entraining admixtures for concrete, American Society for Testing and Materials, Pennsylvania.
[30] ASTM C457, Standard test method for microscopical determination of parameters of the air-void system in hardened concrete, American Society for Testing and Materials, Pennsylvania.